

# Carbon Dots Enabling Parts-Per-Billion Sensitive and Ultraselective Photoluminescence Lifetime-Based Sensing of Inorganic Mercury

Lukáš Zdražil, David Panáček, Veronika Šedajová, Zdeněk Bažura, Michal Langer, Miroslav Medveď, Markéta Paloncýová, Magdalena Scheibe, Sergii Kalytchuk, Giorgio Zoppellaro, Štěpán Kment, Alejandro Cadranel, Aristides Bakandritsos, Dirk M. Guldi, Michal Otyepka, and Radek Zbořil\*

One of the UN Sustainable Development Goals is to ensure universal access to clean drinking water. Among the various types of water contaminants, mercury (Hg) is considered to be one of the most dangerous ones. It is mostly its immense toxicity and vast environmental impact that stand out. To tackle the issue of monitoring water quality, a nanosensor based on carbon dots (CDs) is developed, whose surface is functionalized with carboxylic groups. CDs show Hg<sup>2+</sup> concentration-dependent photoluminescence (PL) lifetimes along with an ultrahigh sensitivity and selectivity. The selectivity of PL quenching by Hg<sup>2+</sup> is rationalized by performing light-induced electron paramagnetic resonance (LEPR) spectroscopy showing significant perturbation of the CD photoexcited state upon Hg<sup>2+</sup> binding. The experimental findings are supported by time-dependent density functional theory (TD-DFT) calculations. These unveiled the emergence of a low-lying charge transfer state involving a vacant 6s orbital of Hg<sup>2+</sup> stabilized by relativistic effects.


## 1. Introduction

One of the world's biggest global challenges is clean and drinkable water. The growing impact of anthropogenic activities (transport, industry, agriculture, and mining)<sup>[1]</sup> exerts an adverse effect on global ecosystems and contributes to the accumulation of toxic heavy metals in the Earth's upper crust.<sup>[2]</sup> This, in turn, renders the availability of quality drinking and sanitary water an increasing concern,<sup>[3]</sup> with several billion people having limited access to clean water (estimated to be around half the population by 2025).<sup>[4]</sup> Therefore, the development of advanced materials and technologies is crucial for an effective on-site remediation and user-friendly water quality monitoring. Among the heavy metals, mercury (Hg) is

L. Zdražil, D. Panáček, V. Šedajová, Z. Bažura, M. Langer, M. Medveď, M. Paloncýová, M. Scheibe, S. Kalytchuk, G. Zoppellaro, Š. Kment, A. Bakandritsos, M. Otyepka, R. Zbořil  
Regional Centre of Advanced Technologies and Materials  
Czech Advanced Technology and Research Institute (CATRIN)  
Palacký University Olomouc  
Šlechtitelů 241/27, Olomouc 783 71, Czech Republic  
E-mail: radek.zboril@upol.cz

L. Zdražil, A. Cadranel, D. M. Guldi  
Department of Chemistry and Pharmacy & Interdisciplinary Center for  
Molecular Materials (ICMM)  
Physical Chemistry I  
Friedrich-Alexander-Universität Erlangen-Nürnberg  
Egerlandstraße 3, 91058 Erlangen, Germany

M. Langer  
Chemical and Biological Systems Simulation Lab  
Centre of New Technologies University of Warsaw  
2c Banacha Street, Warsaw 02-097, Poland  
M. Medveď  
Department of Chemistry  
Faculty of Natural Sciences  
Matej Bel University  
Tajovského 40, Banská Bystrica 974 01, Slovak Republic  
Š. Kment, A. Bakandritsos, R. Zbořil  
Nanotechnology Centre  
Centre for Energy and Environmental Technologies  
VŠB – Technical University of Ostrava  
17. listopadu 2172/15, Ostrava-Poruba 708 00, Czech Republic  
M. Otyepka  
IT4Innovations  
VŠB—Technical University of Ostrava  
17. listopadu 2172/15, Ostrava-Poruba 708 00, Czech Republic

 The ORCID identification number(s) for the author(s) of this article can be found under <https://doi.org/10.1002/adom.202300750>

© 2023 The Authors. Advanced Optical Materials published by Wiley-VCH GmbH. This is an open access article under the terms of the Creative Commons Attribution License, which permits use, distribution and reproduction in any medium, provided the original work is properly cited.

DOI: 10.1002/adom.202300750

certainly the most dangerous, most toxic, most carcinogenic, and most hazardous pollutant.<sup>[5]</sup> Therefore, ultrasensitive Hg sensing is one of the key prerequisites for an effective protection of health and the environment. Hg can be detected by means of a variety of experimental techniques such as cold-vapor atomic fluorescence spectrometry (CV-AFS), inductively coupled plasma-mass spectrometry (ICP-MS), or X-ray absorption spectroscopy (XAS).<sup>[6]</sup> The progress in nanotechnologies has allowed the development of advanced materials enabling Hg detection using different analytical approaches including surface plasmon resonance (SPR),<sup>[7]</sup> surface-enhanced Raman spectroscopy (SERS),<sup>[8]</sup> colorimetric,<sup>[9]</sup> or electrochemical methods.<sup>[10]</sup> Apart from these techniques, PL intensity-based nanosensing Hg remains widely used. In the past, organic dyes<sup>[11]</sup> and luminescent nanomaterials such as gold nanoparticles (Au NPs),<sup>[12]</sup> semiconductor quantum dots (QDs),<sup>[13]</sup> low-dimensional graphitic carbon nitride (g-CN),<sup>[14]</sup> and carbon nanotubes (CNTs)<sup>[15]</sup> were developed for a sensitive Hg detection based on photoluminescence (PL) measurements.

Carbon dots (CDs) represent a relatively new member of the family of carbon-based nanomaterials. CDs exhibit remarkable optical properties, such as broadband optical absorption, strong emission, and good photostability.<sup>[16]</sup> Moreover, due to their small size (<10 nm), high biocompatibility, and bright PL, CDs have attracted considerable interest from researchers worldwide and have been designed for optoelectronics,<sup>[17]</sup> bioimaging,<sup>[18]</sup> drug delivery,<sup>[19]</sup> photocatalysis,<sup>[20]</sup> etc. Additionally, CDs have made it into Hg sensing, where low limits of detection (LODs) are linked to their bright PL, high surface area, and chemically rich shell to bind Hg<sup>2+</sup>.<sup>[21]</sup> Subnanomolar LODs have been achieved using highly emissive fluorophores.<sup>[21d,22]</sup>

Time-consuming calibration of concentration-dependent PL intensity measurements hinders, however, the widespread application of optically active nanomaterials in Hg sensing. In several works, a ratiometric approach for the Hg detection was reported.<sup>[23]</sup> Implicit is the requirement of two luminescent species. This strategy is prone to errors due to fluctuations in the excitation power. Such limitations are overcome by PL lifetime sensing, which in many aspects is superior to both ratiometric and intensity-based measurements. The PL lifetime signal is intrinsically referenced for a broad concentration of analyte, is independent of the probe concentration and inhomogeneity, as well as the intensity of excitation light. It also enables high spatial resolution based on PL lifetime imaging. Yet, despite extensive research in heavy metals detection, sub-ppb level PL lifetime sensing of Hg has not been reported.

In this work, we report on the application of CDs with carboxyl-enriched surface for Hg<sup>2+</sup> sensing in natural water. Hereby, the PL lifetime of CDs was found to depend on the Hg<sup>2+</sup> concentration. PL lifetime measurements allowed accurate determination of ultralow Hg<sup>2+</sup> levels in water. What stands out is their independence from other physical parameters such as pH, ionic strength, and intensity fluctuations of the excitation source. CD-PL-lifetime-based nanosensors showed not only high sensitivity toward Hg<sup>2+</sup> detection with LOD in the sub-ppb region (0.7 ppb), but also high selectivity toward Hg<sup>2+</sup>. Additionally, light-induced electron paramagnetic resonance (LEPR) spec-

troscopy was performed to obtain insights into the selectivity of CD-PL-lifetime-based nanosensors. LEPR studies of the interaction of the photoexcited state of CD with heavy metal ions (Hg<sup>2+</sup>, Cd<sup>2+</sup>, and Pb<sup>2+</sup>) revealed a strong electronic perturbation upon Hg<sup>2+</sup> binding. The experimental observations were corroborated by computational analysis based on molecular dynamics (MD) simulations and time-dependent density functional theory (TD-DFT) calculations. The distinctive sensitivity of CD PL toward Hg<sup>2+</sup> ions is related to their electronic structure, namely a low-lying charge-transfer state involving a relativistically stabilized 6s (Hg<sup>2+</sup>) orbital, that leads to the emergence of CD PL quenching.

## 2. Results and Discussion

Highly luminescent and water-soluble CDs were synthesized by a one-step hydrothermal treatment of citric acid and urea. Detailed structural analysis of the synthesized CDs is described in Figure S1 (Supporting Information). Our results confirm that the synthesized CDs are spherical in shape with an average size of 3.5 nm, and their surface is enriched with carboxyl groups. Mostly, XPS, and FTIR spectroscopies (Figure S1e,f, Supporting Information) lead to these conclusions.

The optical properties of CDs in dilute aqueous suspensions were studied using absorption and PL spectroscopies. PL excitation-emission maps of CDs as shown in Figure 1a prompt to an excitation-independent emission. In particular, the emission peak maxima remain constant over a wide range of excitation wavelengths. This suggests that the PL emission of CDs originates from an excited state that is linked to molecular fluorophores (MFs). CDs exhibited a broad absorption across the visible range with a 335 ± 2 nm maximum. This also supports the occurrence of MFs (Figure 1b, blue curve).<sup>[24,36]</sup> The excitation wavelength range of the CDs extends from 275 to 425 nm, with a maximum excitation occurring at 350 ± 2 nm (Figure 1b, green curve). The PL emission of CDs under excitation at 350 nm (Figure 1b, red curve) is best described as a relatively narrow band with a full width at half-maximum (fwhm) of 66 ± 2 nm and a peak at 445 ± 2 nm. The PL quantum yield (QY) of CDs was determined by the absolute method to be 24 ± 3% under photoexcitation at 350 nm. The PL decay of CDs was studied using time-resolved PL spectroscopy at the 445 nm maximum (Figure 1c). To this end, a PL lifetime of 6.3 ns was extracted using a stretched exponential fitting function (for details see the experimental section in Supporting Information).

Carboxyl and amine groups form strong coordination pockets for toxic metal ions, such as Cd<sup>2+</sup>, Pb<sup>2+</sup>, and Hg<sup>2+</sup>.<sup>[25]</sup> Interactions of heavy metal ions with such high-affinity pockets often result in a sizeable decrease in PL intensity.<sup>[26]</sup> XPS analysis confirmed a significant amount of carboxyl groups on the CD surface. Based on this, we conducted PL intensity measurements varying the Hg<sup>2+</sup> concentration. PL color maps of CDs as they are presented in Figure 1d prompt to a noticeable drop in PL intensity with increasing Hg<sup>2+</sup> concentration (for details see the optical characterization section in Supporting Information). As a matter of fact, for each Hg<sup>2+</sup> concentration all relevant parameters were quantified and summarized in Figure 1e: PL maximum, PL fwhm, and integrated PL intensity.

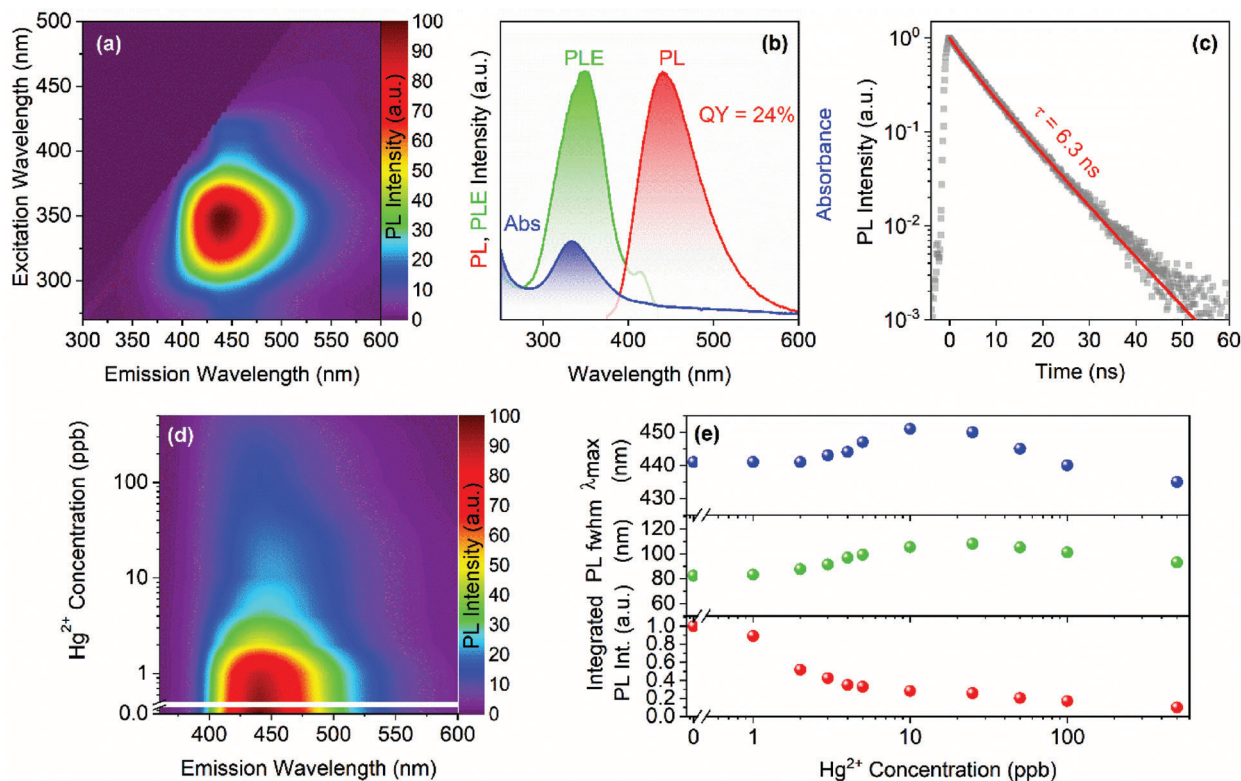


**Figure 1.** Optical characterization of CDs. a) Excitation-emission color map of CDs in diluted aqueous dispersion. b) Absorption (blue curve), normalized PL excitation (green curve,  $\lambda_{em} = 445$  nm) and PL emission spectra (red curve,  $\lambda_{ex} = 350$  nm). c) Time-resolved PL decay ( $\lambda_{em} = 445$  nm) with corresponding stretched exponential fit (red line). d) Color map representing PL emission of CDs in aqueous solutions of  $Hg^{2+}$  with concentrations 0–500 ppb. e) Corresponding  $Hg^{2+}$  concentration-dependent changes in the PL peak maximum  $\lambda_{max}$ , PL fwhm, and normalized integrated PL intensity, respectively.

The PL maximum and the PL fwhm of CDs varied within the interval of 435–455 nm and 83–110 nm, respectively, (Figure 1e, blue and green points). To characterize the nonradiative relaxation processes occurring upon the interaction of  $Hg^{2+}$  with the CDs, the quenching of the integrated PL intensity was analyzed as a function of  $Hg^{2+}$  concentration (Figure 1e, red points). The values of integrated PL intensity were therefore normal-

ized to the intensity of a blank sample such as pure water. They revealed a monotonic decrease as the  $Hg^{2+}$  concentration was increased.

Next, we investigated the PL dynamics of CDs in pure water and in solutions containing 10 ppb and 1 ppm  $Hg^{2+}$ . Time-resolved spectroscopy in the spectral region between 380 and 650 nm is presented in Figure 2a–c. We found that the PL

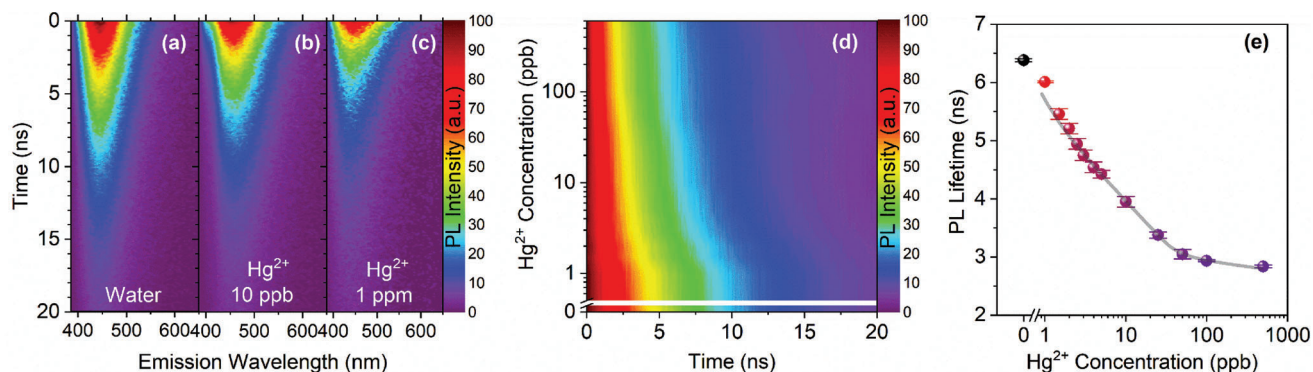


**Figure 2.** Time-resolved  $Hg^{2+}$  concentration-dependent PL emission of CDs. Time-resolved PL emission color maps of CDs in a) pure water, b)  $Hg^{2+}$  solution, 10 ppb, c)  $Hg^{2+}$  solution, 1 ppm. d) Color map of normalized time-resolved PL intensity at the PL emission maximum ( $\lambda_{em} = 445$  nm) versus  $Hg^{2+}$  concentration. e) Extracted PL lifetimes of CDs plotted as a function of  $Hg^{2+}$  concentration (experimental data are given as symbols, whereas the line is the fit by Equation 1; error bars represent the standard deviation from three measurements).

lifetime became shorter and shorter as the  $\text{Hg}^{2+}$  concentration was increased. The spectral shape remained, however, unchanged throughout the different  $\text{Hg}^{2+}$  concentration (Figure 2a–c; Figure S2a, Supporting Information). To investigate the effect of  $\text{Hg}^{2+}$  entrapment on the CD emission dynamics, we derived the radiative ( $\tau_r^{-1}$ ) and nonradiative ( $\tau_{nr}^{-1}$ ) recombination rates of CDs in  $\text{Hg}^{2+}$  solutions of varying concentration. The results revealed a significant rise in  $\tau_{nr}^{-1}$  accompanied with a gradual suppression of  $\tau_r^{-1}$  with increasing  $\text{Hg}^{2+}$  concentration, indicating that the presence of  $\text{Hg}^{2+}$  primarily enhances nonradiative relaxation in CDs (Figure S2b). To exploit these facts for  $\text{Hg}^{2+}$  sensing, we systematically examined the PL lifetime as a function of  $\text{Hg}^{2+}$  concentration (Figure 2d,e). The transient PL color map (Figure 2d) underlines a distinct shortening of the PL lifetimes with increasing  $\text{Hg}^{2+}$  concentration. Every single decay was further fitted using a stretched-exponential fitting function and the extracted PL lifetimes are presented in Figure 2e (details on fitting procedure are described in, Table S1, Supporting Information). PL lifetimes dropped from 6.3 to 2.8 ns as the  $\text{Hg}^{2+}$  concentration was increased from 0 to 500 ppb. The underlying concentration dependence was well described by the following biexponential calibration relationship:

$$c = 0.421 + 50.445 e^{-\frac{\tau-2.926}{0.621}} + 56.001 e^{-\frac{\tau-2.926}{0.063}} \quad (1)$$

where  $c$  is the concentration of  $\text{Hg}^{2+}$  (ppb) and  $\tau$  is the PL lifetime (ns) at  $c$  (ppb). In addition, the LOD was calculated by treating the PL lifetime as a function of  $\text{Hg}^{2+}$  concentration (Figure S3). A value of 0.7 ppb or 3.5 nM is far below the maximum contaminant level (MCL) for inorganic mercury in drinking water of 2 and 6 ppb, as established by the U.S. Environmental Protection Agency (EPA) or the World Health Organization (WHO), respectively. It is also lower than or comparable to previous LODs using PL ratiometric methods (Table S2, Supporting Information).

Ideally, optical nanosensors should be selective, photostable and the optical output for analyte sensing should be independent of other environmental variables like pH, ionic strength, etc. In this context, the selectivity of CD-based nanosensors to-

ward  $\text{Hg}^{2+}$  was demonstrated (Figure 3a). The extracted PL lifetime remained nearly unchanged in the presence of various metal ions. Only the addition of  $\text{Fe}^{2+}$  and  $\text{Fe}^{3+}$  induced visible aggregation of CDs, resulting in longer PL decays (Figure 3; Figure S4, Supporting Information). Additionally, the photostability of CDs was investigated by 38-hour light exposure using a pulsed laser, with an average power of 75  $\mu\text{W}$  and a pulse width of 66.5 ps (Figure S5a,b, Supporting Information). CDs exhibit excellent photostability even after 38 h of continuous photoexcitation. The PL decays at different pH (without the presence of  $\text{Hg}^{2+}$ ) are gathered in Figure S5c,d (Supporting Information). Nearly constant PL lifetimes remained to be seen in the pH range from 3 to 9. Significant changes were, however, discernible in either strongly acidic (pH 1 and pH 2) or basic (pH 10–14) media. Finally, we probed the PL decay in NaCl solutions of varying concentrations (Figure S5e, Supporting Information) without revealing any notable changes at concentrations as high as 1 M NaCl. In other words, CD-based nanosensors operate even in a high ionic strength environment (Figure S5f, Supporting Information).

Motivated by the aforementioned results, we performed time-resolved PL measurements of CD-based nanosensors in natural water samples, that is, tap and mineral water samples to which we have added  $\text{Hg}^{2+}$  (Figure 3b,c). PL decays before (blue line) and after (red line) adding 500 ppb  $\text{Hg}^{2+}$  are presented in Figure 3b,c. The lifetimes of 6.5 versus 1.6 ns validate the capability of CD-based nanosensors to be effective in samples of natural water. As a complement, we looked at drinking water samples containing 1 ppb  $\text{Hg}^{2+}$  (Figure 3d). Here, we confirmed that the sensitivity of the PL lifetime exceeds the MCL of 2 ppb for  $\text{Hg}^{2+}$  even in tap and mineral water samples.

To rationalize the high selectivity in PL quenching in the presence of  $\text{Hg}^{2+}$ , in situ LEPR spectroscopic measurements were conducted. CDs dispersed in water are EPR inactive in the dark (Figure S6a, Supporting Information). Nevertheless, upon photoirradiation (HeCd, @325 nm, 200 mW) spin active species are formed giving rise to an EPR resonant line at  $g = 1.999$  (Figure 4a). The highly asymmetric nature of the EPR signal indicates a distribution of various spin species of diverse nature.

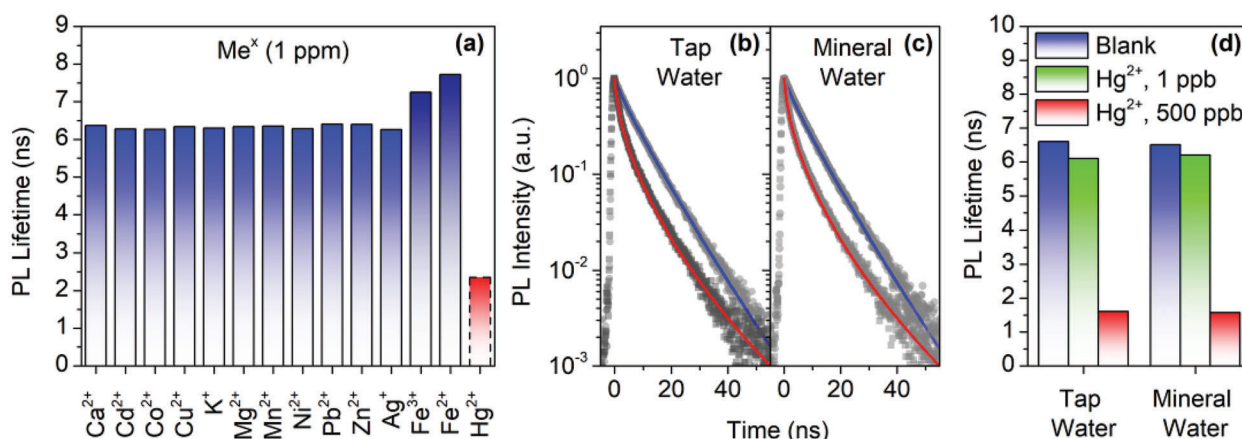


**Figure 3.** Evaluation of selectivity and sensitivity of PL lifetime-based CD-nanosensor in natural water samples. a) Specificity test of CD-sensor for different metal ions (1 ppm). b,c) PL decays, and d) corresponding extracted PL lifetime values of the blank sample (shown in blue), and samples spiked with  $\text{Hg}^{2+}$  ions with concentration of 1 ppb (shown in green), and 500 ppb (shown in red).

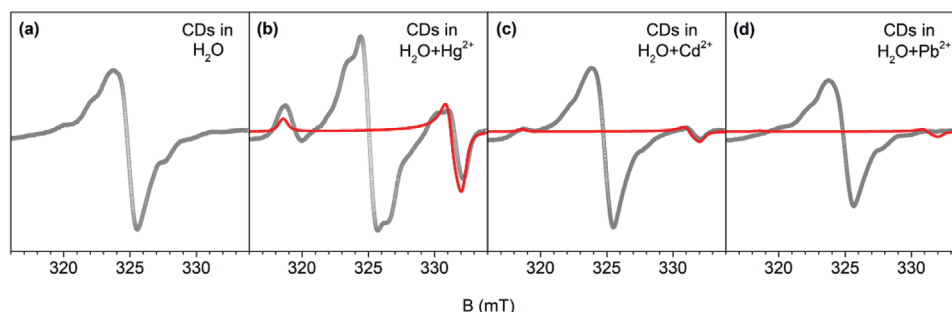


**Figure 4.** Light-induced EPR (LEPR) study of photogenerated spin states at the CD/solvent interface. LEPR envelopes of CDs in a) pure water, b)  $\text{Hg}^{2+}$  solution, c)  $\text{Cd}^{2+}$  solution, and d)  $\text{Pb}^{2+}$  solution. Experimental data are presented as gray symbols, whereas the computer simulations are presented as red lines. Measurements were conducted at  $T = 80$  K and under in situ UV irradiation (@325 nm, 200 mW). Note that in panel (b) the sharp isotropic signal superimposed to the broader signature around 325 mT is associated to a fraction of photoexcited species (spin containing) in which the 6s orbital of the bound  $\text{Hg}^{2+}$  becomes effectively half-filled ( $S = 1/2$ ,  $g \approx 2.00$ ).

They are weakly resonant and develop around an intense resonant line at  $\approx 325$  mT. These signals arise from electron spin moments in CD domains that are rich in  $^{14}\text{N}$  nuclei ( $I = 1$ ) and that couple through hyperfine interactions. Binding diamagnetic  $\text{Hg}^{2+}$  ( $[\text{Xe}] 4f^{14}5d^{10}$ ) retains the EPR silence in the dark (Figure S6b, Supporting Information). Significant changes were noted in the electronic perturbation of the spin active CDs once photoexcited (Figure 4b). Newly formed resonant lines at  $g_x = 2.038$ ,  $g_{y,z} = 1.955$  result from binding  $\text{Hg}^{2+}$  to the CD surface.

Oxygen functionalities such as  $-\text{COOH}$  and  $-\text{COO}^-$  are involved as independently confirmed by FTIR spectroscopy (Figure S7a,b, Supporting Information). For example, the intensity ratio of the carbonyl  $\nu_{\text{C}=\text{O}}$  (above  $1660\text{ cm}^{-1}$ ) and the aromatic  $\nu_{\text{C}=\text{C}}$  (above  $1560\text{ cm}^{-1}$ ) decreased from 1.08 to 0.78 without and with  $\text{Hg}^{2+}$  present. As such, the interaction of  $\text{Hg}^{2+}$  with the carboxyl groups reduces the vibration modes of the carboxyl group.

The EPR experiments prompt to a strong perturbation of the spin active species by the electric field gradient (EFG) stemming from bound  $\text{Hg}^{2+}$ . Effective perturbations of the electron spin moment are gated by an enhanced orbital overlap and spin-orbit-coupling (SOC) effects between the  $\text{Hg}^{2+}$  frontier orbitals and the carboxylate spin-containing sites. Both EPR and FTIR results are in agreement with the literature. CDs that are prepared from citric acid and urea contain MFs based on citrazinic acid derivatives.<sup>[27,36]</sup>  $\text{Hg}^{2+}$  interacts with the carboxyl groups of these MFs when located close to the CD surface. The consequence is a turn-off of PL by an effective EFG-induced electronic perturbation of the spin active species.

Next, we focused on binding other heavy metal pollutants such as  $\text{Cd}^{2+}$  and  $\text{Pb}^{2+}$  and the resulting consequences thereof, especially on the PL quenching. It is worth noting that upon  $\text{Cd}^{2+}$  and  $\text{Pb}^{2+}$  binding, the CD-based nanosensors remained EPR inactive in the dark (Figure S6c,d, Supporting Information). Interestingly, less perturbation is concluded by interacting with  $\text{Cd}^{2+}$  as compared to  $\text{Hg}^{2+}$ . As a matter of fact, the newly formed resonant lines are lower in intensity (Figure 4c). In the case of  $\text{Pb}^{2+}$ , no sizeable changes were observed (Figure 4d). To rule out a preferential  $\text{Hg}^{2+}$  binding to the CD surface over  $\text{Cd}^{2+}$  and  $\text{Pb}^{2+}$  binding, FTIR spectra were recorded. The  $\nu_{\text{C}=\text{O}}/\nu_{\text{C}=\text{C}}$  intensity ratios decreased again from 1.08 to 0.72 in both

cases (Figure S7c,d), indicating an affinity similar to that for  $\text{Hg}^{2+}$ . Overall, our EPR and FTIR results suggest that  $\text{Hg}^{2+}$  ions open nonradiative relaxation channels due to their specific electronic configuration, and, thus, selectively quench the PL in CDs.

Finally, we turned to computational methods to address two important aspects that are linked to metal ion interactions with CDs. On one hand, we explored the preference for specific metal ion binding sites on the CD surface. On the other hand, we analyzed changes in the nature of electronic transitions due to metal ion binding to the MFs in CDs. To this end, we performed MD simulations of urea- and/or carboxyl-functionalized CD layers in the presence of model divalent cations, namely  $\text{Mg}^{2+}$  and  $\text{Hg}^{2+}$ .  $\text{Mg}^{2+}$  was taken as the standard model divalent cation in the MD simulations and the alkaline earth metal counterpart to the transition metal analyte. We considered both neutral and deprotonated CDs albeit only the latter is in line with the aqueous environment used in our experiments. The simulations revealed interactions between  $\text{Mg}^{2+}$  and  $\text{Hg}^{2+}$ , on the one hand, and deprotonated CDs, on the other hand (Figure 5a). Importantly, a significant accumulation of  $\text{Mg}^{2+}$  as well as  $\text{Hg}^{2+}$  was noted in the close proximity of the carboxylate groups (Figures 5b; Figure S14, Supporting Information).<sup>[28]</sup> Higher ionic densities and shorter distances relative to the carboxylate oxygens for  $\text{Hg}^{2+}$  should be highlighted (for details see the Supporting Information). The data confirm that  $\text{Mg}^{2+}$  and  $\text{Hg}^{2+}$  effectively interact with the carboxylates in accordance with the FTIR measurements (Figure S7, Supporting Information). In addition, all-electron relativistic TD-DFT calculations were performed to shed light on the PL quenching by  $\text{Hg}^{2+}$ . We employed the CAM-B3LYP functional,<sup>[29]</sup> the second-order Douglas–Kroll–Hess approach,<sup>[30]</sup> and the quasi-degenerate perturbation theory<sup>[31]</sup> to account for the SOC effects. Solvent effects were included via the Solvation Model based on Density (SMD).<sup>[32]</sup> All calculations were carried out using the Gaussian16<sup>[33]</sup> and ORCA programs.<sup>[34]</sup> Model systems (Figure S9, Supporting Information) consisted of a citrazinate anion (CZA) and  $\text{Hg}^{2+}$ ,  $\text{Cd}^{2+}$ , and  $\text{Pb}^{2+}$ , which gave rise to quite different PL quenching (Figure 3a). A choice of the CZA model was based on the fact that our CDs exhibit excitation-independent emission, which has usually been linked to MFs. The lowest transition ( $S_0 \rightarrow S_1$ ) in CZA is bright with clear  $\pi-\pi^*$  character (Figure S18a, Supporting Information). Despite the close vicinity of

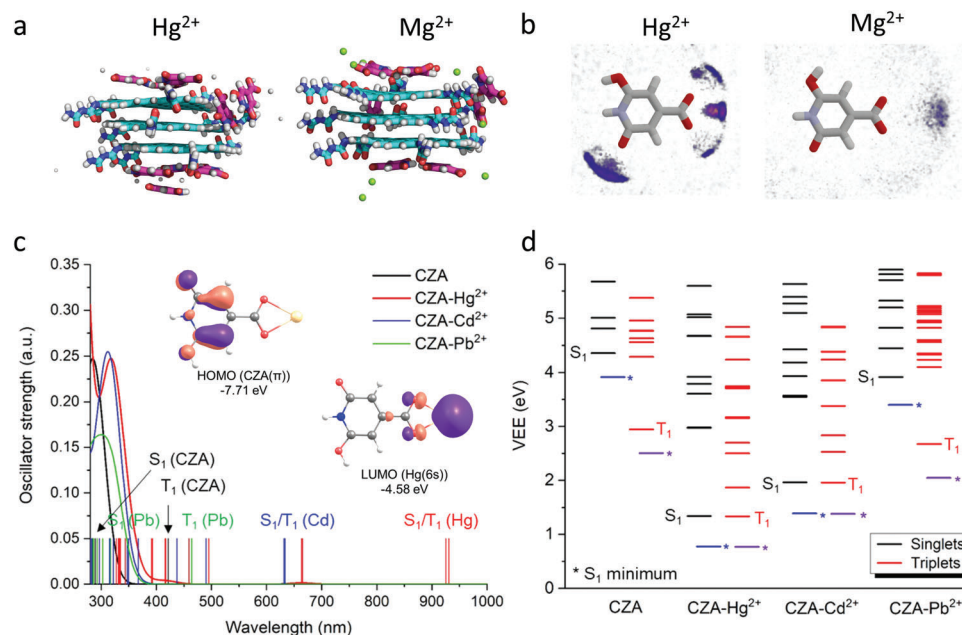


**Figure 5.** Computational analysis of the interactions of metal cations with CDs/MFs. a) Final structures of self-assembly MD simulations of urea-functionalized CD layers (cyan) with MFs (magenta) in the presence of  $\text{Hg}^{2+}$  and  $\text{Mg}^{2+}$  cations (white and green balls). Water and chlorides are omitted for clarity. b) Structures of a citrazinate anion (CZA) and the density distribution of  $\text{Hg}^{2+}$  and  $\text{Mg}^{2+}$  ions calculated from MD simulations showing the accumulation of cations around the carboxylate group. c) Absorption spectra of CZA (black) and its complexes with  $\text{Hg}^{2+}$  (red),  $\text{Cd}^{2+}$  (blue), and  $\text{Pb}^{2+}$  (green) cations. Sticks indicate the position of transitions as revealed by the relativistic TD-DFT calculations including SOC effects. Inset: HOMO and LUMO involved in the  $S_0 \rightarrow S_1$  transition of CZA- $\text{Hg}^{2+}$ . d) Energy level diagram showing the position of singlet (black/blue) and triplet (red/violet) excited states of CZA and its complexes. The levels with an asterisk correspond to the optimized  $S_1$  structures. Color coding for displayed structures: carbon – grey, nitrogen – blue, oxygen – red, hydrogen – white, and mercury – yellow.

singlet and triplet energy levels (Figure S18b, Supporting Information), the probability of intersystem crossing (ISC) is very low (SOC:  $0.02 \text{ cm}^{-1}$ ). Consequently, CZAs emerge as strongly emissive.  $\text{Hg}^{2+}$  binding changes the picture. A new low-energy level associated with the low-lying vacant 6s orbital of  $\text{Hg}^{2+}$  emerges. It is known to be stabilized by relativistic effects.<sup>[35]</sup> This new charge-transfer state (CZA  $\pi \rightarrow \text{Hg}^{2+} 6s$ ), which is only 0.77 eV above the ground state (Figures 5c; Figure S19, Supporting Information), can effectively contribute to the PL quenching. In stark contrast, the HOMOs of  $\text{Cd}^{2+}$  and  $\text{Pb}^{2+}$  corresponding to 5s and 6p orbitals, respectively, have higher energies than the 6s orbital of  $\text{Hg}^{2+}$ . Energies of 1.38 and 3.34 eV render a radiationless deactivation less likely (Figures 5d; Figures S20 and S21, Supporting Information). PL quenching in CDs in the presence of  $\text{Hg}^{2+}$  is yet another demonstration of relativistic effects in chemistry.

### 3. Conclusion

In this study, we present the synthesis and characterization of the first carboxyl-rich CDs based mercury sensor with a PL decay that is highly dependent on  $\text{Hg}^{2+}$  concentrations. Our CD-based nanosensors display a turn-off PL lifetime and a remarkable degree of selectivity toward  $\text{Hg}^{2+}$ . These properties were of key importance to achieve highly accurate, ppb sensitive, and self-referenced  $\text{Hg}^{2+}$  sensing in water. As such, we demonstrated a

LOD of 0.7 ppb (3.5 nm) and a record selectivity toward  $\text{Hg}^{2+}$ . Additionally, CDs show high resistance to photobleaching and remain stable even under continuous pulsed laser excitation for up to 38 h. Likewise, their properties remain invariant upon changes in pH and ionic strength. Moreover, with a low cost of precursors (0.14 EUR per reaction), the presented method offers considerable commercial potential.

We also showcase the vast potential of CDs for  $\text{Hg}^{2+}$  sensing in drinking water through two case studies using tap and mineral water. Our CD-based nanosensors are capable of operating at  $\text{Hg}^{2+}$  concentrations as low as 1 ppb, which is below the MCL for  $\text{Hg}^{2+}$  for drinking water established by the U.S. Environmental Protection Agency (2 ppb) and the World Health Organization (6 ppb), demonstrating their commercial utility in natural water samples. As a complement, we investigated the selectivity of PL quenching with  $\text{Hg}^{2+}$  experimentally by LEPR spectroscopy and theoretically by computational analysis. Our results underline the significant perturbations of the CD photoexcited state upon interactions with  $\text{Hg}^{2+}$ . Our investigations extend the use of CDs in  $\text{Hg}^{2+}$  detection beyond standard concentration-dependent PL intensity and PL ratiometric methods, providing a fundamental understanding of the underlying detection mechanism.

### Supporting Information

Supporting Information is available from the Wiley Online Library or from the author.

## Acknowledgements

The work was supported by the ERDF/ESF project "Nano4Future" (No. CZ.02.1.01/0.0/0.0/16\_019/0000754). R.Z. and A.B. acknowledge the funding from the Czech Science Foundation, GA CR – EXPRO, 19–27454X. M.O., V.Š., and D.P. acknowledges the funding from the European Union's Horizon Europe research and innovation programme under grant agreement No. 101059266. Operation of XPS and TEM facilities was partly funded by the Research Infrastructure NanoEnviCz, supported by the Ministry of Education, Youth and Sports of the Czech Republic under Project No. LM2018124. M.M. acknowledges the support of the Slovak Research and Development Agency (APVV-20-0098). The COST Action CA21101 is also acknowledged. Ms. Jana Stráská is acknowledged for TEM characterization of samples. Mr. Lukáš Tabery is acknowledged for support in optical measurements. This work was supported by the Ministry of Education, Youth and Sports of the Czech Republic through the e-INFRA CZ (ID: 90254). M.O. acknowledges support by the project "Experimental and theoretical studies of near-infrared-emitting and chiral carbon dot luminescence" funded by Moravian-Silesian Region and VSB-TUO, contract nr. 00734/2023/RRC. D.G. acknowledges the support from "Solar Technologies go Hybrid" an initiative from the free state of Bavaria.

## Conflict of Interest

The authors declare no conflict of interest.

## Data Availability Statement

The data that support the findings of this study are available from the corresponding author upon reasonable request.

## Keywords

carbon dots, colloidal nanomaterials, mercury sensing, time-resolved photoluminescence

Received: March 29, 2023

Revised: May 12, 2023

Published online:

- [1] S. Bolisetty, R. Mezzenga, *Nat. Nanotechnol.* **2016**, *11*, 365.
- [2] J. O. Nriagu, *Science* **1996**, *272*, 223.
- [3] Sustainable Development Knowledge Platform (United Nations), <https://sustainabledevelopment.un.org> (accessed: March 2022)
- [4] (WHO) Fact Sheet on Water: Key Facts, Water and Health, [https://water.org/documents/223/FY22\\_Key\\_Water.org\\_facts.pdf](https://water.org/documents/223/FY22_Key_Water.org_facts.pdf) (accessed: June 2022).
- [5] S. Ali, M. Mansha, N. Baig, S. A. Khan, *Chem. Rec.* **2022**, *22*, e202100327.
- [6] N. Logan, J. Lou-Franco, C. Elliott, C. Cao, *Environ. Sci.-Nano* **2021**, *8*, 2718.
- [7] a) T. Xue, K. Qi, C. Hu, *Sens. Actuators B* **2019**, *284*, 589; b) B. Janani, A. Syed, A. M. Thomas, N. Marraiki, S. Al-Rashed, A. M. Elgorban, L. L. Raju, A. Das, S. S. Khan, *J. Mol. Liq.* **2020**, *311*, 113281; c) L. Liu, K. Ye, C. Lin, Z. Jia, T. Xue, A. Nie, Y. Cheng, J. Xiang, C. Mu, B. Wang, F. Wen, K. Zhai, Z. Zhao, Y. Gong, Z. Liu, Y. Tian, *Nat. Commun.* **2021**, *12*, 3870.
- [8] W. Ma, M. Sun, L. Xu, L. Wang, H. Kuang, C. Xu, *Chem. Commun.* **2013**, *49*, 9006.
- [9] a) Y. Wang, F. Yang, X. Yang, *ACS Appl. Mater. Interfaces* **2010**, *2*, 339; b) Y. Wang, F. Yang, X. Yang, *Biosens. Bioelectron.* **2010**, *25*, 1994; c) C. C. Huang, H. T. Chang, *Chem. Commun.* **2007**, *12*, 1215; d) Y. Zhu, Y. Cai, Y. Zhu, L. Zheng, J. Ding, Y. Quan, L. Wang, B. Qi, *Biosens. Bioelectron.* **2015**, *69*, 174.
- [10] a) H. Khani, M. K. Rofouei, P. Arab, V. K. Gupta, Z. Vafaei, *J. Hazard. Mater. Mater.* **2010**, *183*, 402; b) P. Li, D. Zhang, C. Jiang, X. Zong, Y. Cao, *Biosens. Bioelectron.* **2017**, *98*, 68.
- [11] a) X. Guo, X. Qian, L. Jia, *J. Am. Chem. Soc.* **2004**, *126*, 2272; b) J. Du, J. Fan, X. Peng, P. Sun, J. Wang, H. Li, S. Sun, *Org. Lett.* **2010**, *12*, 476; c) A. Ono, H. Togashi, *Angew. Chem.* **2004**, *116*, 4400; d) J. Wang, B. Liu, *Chem. Commun.* **2008**, *39*, 4759; e) R. Métivier, I. Leray, B. Lebeau, B. Valeur, *J Mater Chem* **2005**, *15*, 2965.
- [12] a) J. Xie, Y. Zheng, J. Y. Ying, *Chem. Commun.* **2010**, *46*, 961; b) H. Wei, Z. Wang, L. Yang, S. Tian, C. Hou, Y. Lu, *Analyst* **2010**, *135*, 1406; c) L. Shang, L. Yang, F. Stockmar, R. Popescu, V. Trouillet, M. Bruns, D. Gerthsen, G. U. Nienhaus, *Nanoscale* **2012**, *4*, 4155; d) C.-C. Huang, Z. Yang, K.-H. Lee, H.-T. Chang, *Angew. Chem.* **2007**, *46*, 6824; e) D. Hu, Z. Sheng, P. Gong, P. Zhang, L. Cai, *Analyst* **2010**, *135*, 1411.
- [13] a) Y. S. Xia, C. Q. Zhu, *Talanta* **2008**, *75*, 215; b) M. Li, Q. Wang, X. Shi, L. A. Hornak, N. Wu, *Anal. Chem.* **2011**, *83*, 7061; c) B. Zhang, H. Meng, X. Wang, H. Chang, W. Wei, *Sens. Actuators B* **2017**, *253*, 495.
- [14] a) S. Barman, M. Sadhukhan, *J Mater Chem* **2012**, *22*, 21832; b) Q. Wang, W. Wang, J. Lei, N. Xu, F. Gao, H. Ju, *Anal. Chem.* **2013**, *85*, 12182.
- [15] L. Zhang, T. Li, B. Li, J. Li, E. Wang, *Chem. Commun.* **2010**, *46*, 1476.
- [16] a) S. Y. Lim, W. Shen, Z. Gao, *Chem. Soc. Rev.* **2015**, *44*, 362; b) L. Wang, W. Li, L. Yin, Y. Liu, H. Guo, J. Lai, Y. Han, G. Li, M. Li, J. Zhang, R. Vajtai, P. M. Ajayan, M. Wu, *Sci. Adv.* **2020**, *6*, eabb6772; c) B. Wang, S. Lu, *Matter* **2022**, *5*, 110; d) G. Ragazzon, A. Cadranell, E. V. Ushakova, Y. Wang, D. M. Guldi, A. L. Rogach, N. A. Kotov, M. Prato, *Chem* **2021**, *7*, 606.
- [17] a) L. Zdražil, S. Kalytchuk, K. Holá, M. Petr, O. Zmeškal, Š. Kment, A. L. Rogach, R. Zbořil, *Nanoscale* **2020**, *12*, 6664; b) F. Yuan, Y.-K. Wang, G. Sharma, Y. Dong, X. Zheng, P. Li, A. Johnston, G. Bappi, J. Z. Fan, H. Kung, B. Chen, M. I. Saidaminov, K. Singh, O. Voznyy, O. M. Bakr, Z.-H. Lu, E. H. Sargent, *Nat. Photonics* **2019**, *14*, 171; c) S. Kalytchuk, L. Zdražil, M. Scheibe, R. Zbořil, *Nanoscale* **2020**, *12*, 8379; d) Y. Chen, M. Zheng, Y. Xiao, H. Dong, H. Zhang, J. Zhuang, H. Hu, B. Lei, Y. Liu, *Adv. Mater.* **2016**, *28*, 312; e) B. Zhao, Z. Wang, Z. a. Tan, *Nat. Photonics* **2020**, *14*, 130.
- [18] a) M. Zheng, S. Ruan, S. Liu, T. Sun, D. Qu, H. Zhao, Z. Xie, H. Gao, X. Jing, Z. Sun, *ACS Nano* **2015**, *9*, 11455; b) X. Huang, F. Zhang, L. Zhu, K. Y. Choi, N. Guo, J. Guo, K. Tackett, P. Anilkumar, G. Liu, Q. Quan, H. S. Choi, G. Niu, Y.-P. Sun, S. Lee, X. Chen, *ACS Nano* **2013**, *7*, 5684; c) S. Zhu, J. Zhang, C. Qiao, S. Tang, Y. Li, W. Yuan, B. Li, L. Tian, F. Liu, R. Hu, H. Gao, H. Wei, H. Zhang, H. Sun, B. Yang, *Chem. Commun.* **2011**, *47*, 6858; d) D. Li, P. Jing, L. Sun, Y. An, X. Shan, X. Lu, D. Zhou, D. Han, D. Shen, Y. Zhai, S. Qu, R. Zbořil, A. L. Rogach, *Adv. Mater.* **2018**, *30*, 1705913.
- [19] a) W.-Q. Li, Z. Wang, S. Hao, L. Sun, M. Nisic, G. Cheng, C. Zhu, Y. Wan, L. Ha, S.-Y. Zheng, *Nanoscale* **2018**, *10*, 3744; b) T. Feng, X. Ai, G. An, P. Yang, Y. Zhao, *ACS Nano* **2016**, *10*, 4410; c) J. Tang, B. Kong, H. Wu, M. Xu, Y. Wang, Y. Wang, D. Zhao, G. Zheng, *Adv. Mater.* **2013**, *25*, 6569.
- [20] a) K. Holá, M. V. Pavliuk, B. Németh, P. Huang, L. Zdražil, H. Land, G. Berggren, H. Tian, *ACS Catal.* **2020**, *10*, 9943; b) B. Jana, Y. Reva, T. Scharl, V. Strauss, A. Cadranell, D. M. Guldi, *J. Am. Chem. Soc.* **2021**, *143*, 20122; c) Q. Wu, J. Cao, X. Wang, Y. Liu, Y. Zhao, H. Wang, Y. Liu, H. Huang, F. Liao, M. Shao, Z. Kang, *Nat. Commun.* **2021**, *12*, 483; d) L. Zdražil, Z. Bad'ura, M. Langer, S. Kalytchuk, D. Panáček, M. Scheibe, Š. Kment, H. Kmentová, M. A. Thottappali, E. Mohammadi, M. Medveď, A. Bakandritsos, G. Zoppellaro, R. Zbořil, M. Otyepka, *Small* **2023**, e2206587.

- [21] a) L. Zhou, Y. Lin, Z. Huang, J. Ren, X. Qu, *Chem. Commun.* **2012**, 48, 1147; b) R. Zhang, W. Chen, *Biosens. Bioelectron.* **2014**, 55, 83; c) F. Yan, Y. Zou, M. Wang, X. Mu, N. Yang, L. Chen, *Sens. Actuators B* **2014**, 192, 488; d) W. Lu, X. Qin, S. Liu, G. Chang, Y. Zhang, Y. Luo, A. M. Asiri, A. O. Al-Youbi, X. Sun, *Anal. Chem.* **2012**, 84, 5351; e) X. Cui, L. Zhu, J. Wu, Y. Hou, P. Wang, Z. Wang, M. Yang, *Biosens. Bioelectron.* **2015**, 63, 506; f) H. Qi, X. Sun, T. Jing, J. Li, J. Li, *RSC Adv.* **2022**, 12, 1989.
- [22] H. Tan, B. Liu, Y. Chen, *ACS Nano* **2012**, 6, 10505.
- [23] a) X. Zhang, Y. Xiao, X. Qian, *Angew. Chem.* **2008**, 47, 8025; b) Q. Liu, J. Peng, L. Sun, F. Li, *ACS Nano* **2011**, 5, 8040; c) D. Cheng, W. Zhao, H. Yang, Z. Huang, X. Liu, A. Han, *Tetrahedron Lett.* **2016**, 57, 2655; d) Y. Zhou, X. He, H. Chen, Y. Wang, S. Xiao, N. Zhang, D. Li, K. Zheng, *Sens. and Actuators B-Chem.* **2017**, 247, 626; e) Y. Ge, A. Liu, R. Ji, S. Shen, X. Cao, *Sens. Actuators B* **2017**, 251, 410; f) J. Ma, Y. Xiao, C. Zhang, M. Zhang, Q. Wang, W. Zheng, S. Zhang, *Mater. Sci. Eng. B* **2020**, 259, 114582; g) S. Subedi, L. N. Neupane, H. Yu, K.-H. Lee, *Sens. Actuators B* **2021**, 338, 129814; h) X. Jiao, C. Liu, S. He, L. Zhao, X. Zeng, *Dyes Pig.* **2019**, 160, 86; i) M. H. Yang, P. Thirupathi, K. H. Lee, *Org. Lett.* **2011**, 13, 5028; j) J. Hu, Z. Hu, S. Liu, Q. Zhang, H.-W. Gao, K. Uvdal, *Sens. Actuators B* **2016**, 230, 639; k) Y.-Y. Lv, W. Gu, J.-B. Wang, W.-B. Huang, W.-X. Shen, X.-Y. Sun, *Sens. Actuators B* **2017**, 246, 1017; l) W. Xuan, C. Chen, Y. Cao, W. He, W. Jiang, K. Liu, W. Wang, *Chem. Commun.* **2012**, 48, 7292; m) A. Manna, D. Sarkar, S. Goswami, C. K. Quah, H.-K. Fun, *RSC Adv.* **2016**, 6, 57417; n) F. Yarur, J.-R. Macairan, R. Naccache, *Environ. Sci.-Nano* **2019**, 6, 1121; o) S. Mohandoss, H. D. Khanal, S. Palanisamy, S. You, J. J. Shim, Y. R. Lee, *Anal. Methods* **2022**, 14, 635; p) T. Li, X. Li, Y. Zheng, P. Zhu, C. Zhang, K. Zhang, J. J. Xu, *Anal. Chem.* **2023**, 95, 2445.
- [24] a) W. Kasprzyk, T. Swiergosz, S. Bednarz, K. Walas, N. V. Bashmakova, D. Bogdal, *Nanoscale* **2018**, 10, 13889; b) S. Kalytchuk, L. Zdražil, Z. Bad'ura, M. Medved, M. Langer, M. Paloncayova, G. Zoppellaro, S. V. Kershaw, A. L. Rogach, M. Otyepka, R. Zbořil, *ACS Nano* **2021**, 15, 6582; c) V. Strauss, H. Wang, S. Delacroix, M. Ledendecker, P. Wessig, *Chem. Sci.* **2020**, 11, 8256.
- [25] a) Y. Peng, H. Huang, Y. Zhang, C. Kang, S. Chen, L. Song, D. Liu, C. Zhong, *Nat. Commun.* **2018**, 9, 187; b) J. Kolařík, A. Bakandritsos, Z. Bad'ura, R. Lo, G. Zoppellaro, Š. Kment, A. Naldoni, Y. Zhang, M. Petr, O. Tomanec, J. Filip, M. Otyepka, P. Hobza, R. Zboril, *ACS Nano* **2021**, 15, 3349.
- [26] D. Panáček, L. Zdražil, M. Langer, V. Šedajova, Z. Badura, G. Zoppellaro, Q. Yang, E. P. Nguyen, R. Alvarez-Diduk, V. Hrubý, J. Kolařík, N. Chalmes, A. B. Bourlinos, R. Zbořil, A. Merkoci, A. Bakandritsos, M. Otyepka, *Small* **2022**, 33, 2201003.
- [27] W. Kasprzyk, T. Swiergosz, P. P. Romanczyk, J. Feldmann, J. K. Stolarczyk, *Nanoscale* **2022**, 14, 14368.
- [28] a) R. Skanberg, M. Falk, M. Linares, A. Ynnerman, I. Hotz, *IEEE Trans Vis Comput Graph* **2022**, 28, 3126; b) R. Skánberg, C. König, P. Norman, M. Linares, D. Jönsson, I. Hotz, A. Ynnerman, in *Workshop on Molecular Graphics and Visual Analysis of Molecular Data* (Eds.: J. Byska, M. Krone, B. Sommer), The Eurographics Association, Saarbrücken, Germany **2018**.
- [29] a) T. Yanai, D. P. Tew, N. C. Handy, *Chem. Phys. Lett.* **2004**, 393, 51; b) A. D. Becke, *J. Chem. Phys.* **1993**, 98, 5648.
- [30] a) M. Douglas, N. M. Kroll, *Ann. Phys.* **1974**, 82, 89; b) B. A. Hess, *Phys. Rev. A* **1986**, 33, 3742; c) T. Nakajima, K. Hirao, *Chem. Rev.* **2012**, 112, 385.
- [31] B. de Souza, G. Farias, F. Neese, R. Izsak, *J. Chem. Theory Comput.* **2019**, 15, 1896.
- [32] A. V. Marenich, C. J. Cramer, D. G. Truhlar, *J. Phys. Chem. B* **2009**, 113, 6378.
- [33] M. J. Frisch, G. W. Trucks, H. B. Schlegel, G. E. Scuseria, M. A. Robb, J. R. Cheeseman, G. Scalmani, V. Barone, G. A. Petersson, H. Nakatsuji, X. Li, M. Caricato, A. V. Marenich, J. Bloino, B. G. Janesko, R. Gomperts, B. Mennucci, H. P. Hratchian, J. V. Ortiz, A. F. Izmaylov, J. L. Sonnenberg, D. Williams-Young, F. Ding, F. Lipparini, F. Egidi, J. Goings, B. Peng, A. Petrone, T. Henderson, D. RanaOchtereski, et.al. Gaussian 16, Revision B.01, Gaussian Inc, Wallingford, CT, **2016**.
- [34] a) F. Neese, *Wiley Interdiscip. Rev. : Comput. Mol. Sci.* **2011**, 2, 73; b) F. Neese, *Wiley Interdiscip. Rev. : Comput. Mol. Sci.* **2017**, 8, e1352.
- [35] P. Pykkö, *Annu. Rev. Phys. Chem.* **2012**, 63, 45.
- [36] W. Wang, B. Wang, H. Embrechts, C. Damm, A. Cadranel, V. Strauss, M. Distaso, V. Hinterberger, D. M. Guldi, W. Peukert, *RSC Adv.* **2017**, 7, 24771.